ELSEVIER

Computers and Chemical Engineering 26 (2002) 227–237

Computers & Chemical Engineering

www.elsevier.com/locate/compchemeng

Large-scale dynamic optimization for grade transitions in a low density polyethylene plant

A.M. Cervantes [b], S. Tonelli [a], A. Brandolin [a], J.A. Bandoni [a], L.T. Biegler [b,*]

[a] *Planta Piloto de Ingenieria Química, PLAPIQUI (UNS-CONICET), Camino La Carrindanga Km. 7, 8000 Bahía Blanca, Argentina*
[b] *Chemical Engineering Department, Carnegie Mellon University, Pittsburgh, PA 15213-3890, USA*

Received 17 October 2000; received in revised form 21 August 2001; accepted 21 August 2001

Abstract

This paper presents the optimal control policy of an industrial low-density polyethylene (LDPE) plant. Based on a dynamic model of the whole plant, optimal feed profiles are determined to minimize the transient states generated during the switching between different steady states. The industrial process under study produces LDPE by high-pressure polymerization of ethylene in a tubular reactor using oxygen and organic peroxides as initiators. The plant produces polyethylene of different grades that require continuous changes from one steady state to another, in order to switch among the different final products. These changes generate disturbances that keep the product out of specifications during the transient states, with a consequent economic loss. The plant model consists of two parts; the first one corresponds to the tubular reactor. Here, the partial differential equations corresponding to the mass and energy dynamic balances are discretized along the distance coordinate by using finite differences. The resulting ordinary differential equations include the energy balance and individual mass balances for oxygen, peroxides, ethylene, butane, free radicals and polymer. Although, methane is also present in the plant, in the reactor model it is considered as a nonreacting impurity along with the other impurities coming from the rest of the process. The second part of the model corresponds to the rest of the plant. Here we considered four components: ethylene, butane, methane and impurities. An interesting aspect of this process is the presence of many time delays that are incorporated in the optimization model. The resulting differential algebraic equation (DAE) plant model includes over five hundred equations. The dynamic optimization problem is solved using a simultaneous nonlinear programming (NLP) approach. The continuous state and control variables are discretized, by applying orthogonal collocation on finite elements. The resulting NLP is solved with a reduced space Interior Point Algorithm, which is applied directly to the NLP. In addition, a new mesh refinement strategy is applied to this model to confirm that no further improvement can be found in the optimal control profiles. The paper studies two cases of switching among different polymer grades, determining the optimal profiles of butane fed to the plant, in order to minimize the time to reach the steady state operation corresponding to the desired new product quality. The results are also compared with simpler model where reactor was considered as a black-box with the conversion level taken as constant data for each polymer grade. As a result, the dynamic model we developed and the solution methodology used is a flexible and practical tool to help process engineers for taking decisions during the plant operation.

Keywords: Low-density polyethylene; Dynamic optimization; High-pressure polymerization

1. Introduction

The production of low-density polyethylene (LDPE) is a typical process where unsteady states are part of the normal operation of the plant. To obtain LDPE of different grades, in addition to the normal disturbances of any process, programmed variations are originated when operators change product specifications, by switching between different steady states. During the transient periods the plant produces off specification products with a consequent economic loss. This loss could be decreased if the plant operators would use profiles for the manipulated variables that are obtained through an optimization procedure. Different optimization objectives could be used in order to find these

* Corresponding author. Tel.: +1-412-268-2232; fax: +1-412-268-7139.
E-mail address: biegler@andrew.cmu.edu (L.T. Biegler).

0098-1354/02/$ - see front matter
PII: S0098-1354(01)00743-8

optimal trajectories, where a common performance criterion is the difference between the current profile and the new desired steady state. In order to deal with this type of problem in a systematic way, it is necessary to develop and optimize an adequate dynamic model for the process with the right objective function.

In this work, we develop a dynamic model for the entire plant, based on a reformulation of a nonlinear model for the plant (Schbib, Tonelli, Brignole, & Romagnoli, 1992), and a dynamic version of a rigorous steady-state reactor model developed by Brandolin, Lacunza, Ugrin, and Capiati, 1996. The whole model is posed as a dynamic optimization problem to obtain optimal profiles for manipulated variables. The dynamic optimization problem is transformed into a Nonlinear Programming Problem (NLP) by applying collocation on finite elements, and the resulting NLP problem is solved with a novel, recently developed interior point strategy, applied in the reduced space.

The paper is organized as follows. In the next section, we present a brief description of the LDPE process and a detailed explanation of the process models. Section 3 describes the solution procedure, while results are presented in Section 4. Conclusions and future directions are described in Section 5.

2. LDPE process description and model

2.1. Process description

The industrial process under study produces LDPE by high-pressure polymerization of ethylene in a tubular reactor, using gaseous oxygen and organic peroxides as initiators. The plant considered has a nominal capacity of 90,000 tons per year. Fig. 1 shows the plant flowsheet and typical operating conditions. The fresh ethylene feed is mixed with a purified low-pressure recycle stream, oxygen and a chain-transfer agent (butane), and then compressed till about 250 bars in a multi-stage primary compressor. This stream is mixed with the high-pressure recycle, further compressed in a hypercompressor up to the reaction pressure of around 2000 bars, and continuously fed to a jacketed tubular reactor, where the ethylene is partially polymerized, producing polyethylene of different grades. Two additional feeds of organic peroxide are allocated at two different axial positions, producing two reaction zones with sharp temperature and conversion increases.

The ethylene–polymer mixture from the reactor output is expanded through a special letdown valve and fed to a series of high–low pressure separators where the polymer is obtained. The ethylene is cooled and dewaxed prior to being recycled. The polymer is obtained from the low-pressure separator and fed into an extruder to be pelleted, cooled and finally sent to storage.

During normal operation, the plant requires continuous changes from one steady state to another in order to switch among different final products. This can be accomplished by changing the butane feed flow rate and/or the purge flow rate from the precompressor. These changes generate disturbances that keep the product out of specification during the transient states.

2.2. Plant model

The plant model includes four components: ethylene ($j=1$), butane ($j=2$), methane ($j=3$) and impurities ($j=4$). This last component groups several components present in minor quantities.

During the usual plant operation the equipment temperature and pressure are strictly controlled. Therefore, their variations are not significant. For this reason, the momentum and energy balances were not taken into account in the overall plant model. Based on the realistic assumption that the dynamics of the total mass balances is much faster than that of the component mass balances, constant equipment holdups are considered. This model was also verified in dynamic plant tests (Schbib et al., 1992).

Each process unit of the flowsheet was represented as a continuous stirred tank (CST). Nonsteady state mass balances for three components are developed while the fourth component is obtained by difference. Eq. (1) shows the corresponding balance for the jth component:

$$\frac{\mathrm{d}(V\rho w^j)}{\mathrm{d}t} = Fw_{\mathrm{i}}^j - Fw^j \quad j=1,\ldots,3 \tag{1}$$

where F, mass flowrate (kg/h); V, equipment volume (m^3); t, time (s); ρ, gas density (kg/m^3); w_{i}^j, inlet weight component of jth component; w^j, outlet weight component of jth component.

Another aspect of this process is the presence of several time delays. In preliminary work (Cervantes, Tonelli, Bandoni, & Biegler, 1998), a first order Padé approximation in the space of state variables was used to model the delays, and incorporated in the plant model. In this work, a different and tighter method is applied for the time delay prediction.

Here time delays are directly incorporated into the plant model by considering each one as a tube of length L where a plug flow is assumed. The resulting component material balances for these tubes are as follows:

$$\frac{\partial w^j}{\partial t} + \frac{F}{\rho A}\frac{\partial w^j}{\partial z} = 0 \tag{2}$$

$$\left.\frac{\partial w^j}{\partial z}\right|_L = 0; \quad w^j(z,0) = w_0^j,$$

where A is transversal area (m^2); z, axial length (m).

These partial differential equations are discretized using a backward difference equation in z, with $N = 10$ intervals.

In order to avoid a prohibitively large number of difference equations, a dynamic analysis of the process behavior was performed and the many delays present in the whole plant were lumped into only six time delays. The global dynamic plant behavior was retained by an appropriate selection of the location for the six time delays.

2.3. Reactor model

The dynamic model for the reactor was built on the basis of a rigorous mathematical model for the steady-state high-pressure polymerization of ethylene in industrial tubular reactors, previously developed by Brandolin et al. (1996). The rigorous model considers multiple monomer feeds and multiple injections of initiators and chain transfer agents at different locations through the axial length, along with realistic jacket flux configurations. The model is based on the following basic hypothesis: a plug flow reaction mixture forming a single supercritical phase and variation of all physical and transport properties along the axial distance. En-

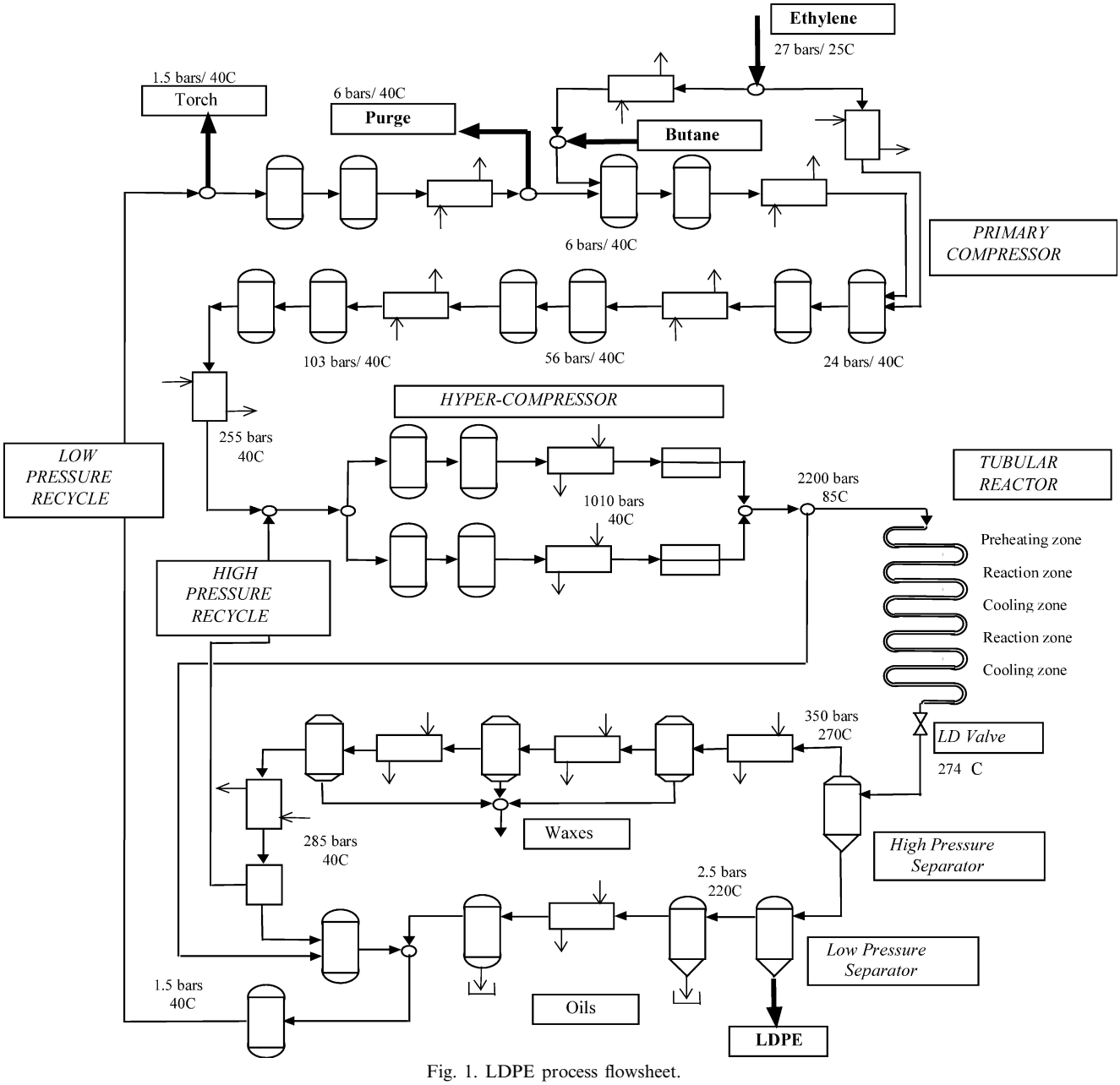

Fig. 1. LDPE process flowsheet.

ergy and momentum balances were implemented to obtain the corresponding equations for temperature and pressure at the reaction side. Pulsed flow operation was also included in the model.

Correlations obtained with experimental data were used to determine global heat transfer coefficients according to Lacunza, Ugrin, Capiati, and Brandolin, (1998). Rigorous mass balances were implemented for ethylene monomer, initiators, telogens, inerts, and moments of the chain-length distributions of radicals and polymer. The energy and momentum balances that account for variations of jacket temperatures and pressures were also included. Some of the kinetic constants were taken from the literature data while the others were used as adjustable parameters to fit experimental data. The whole reaction mechanism and the set of differential–algebraic equations evolved from the mass, momentum and energy balances are described in Brandolin et al. (1996). This model has been validated with experimental data as well, both in steady state and through dynamic pulse testing. The model consists of the following items as a function of axial distance: monomer conversion, reaction and jacket temperatures, reaction and jacket pressures, mass fraction of: oxygen, peroxide initiators, monomer, radicals and polymer, along with the first three moments for the combined length and branching distributions of radicals and polymer; thermodynamic and transport properties of the reaction mixture; average molecular weights and molecular weight distribution (MWD); short and long chain branching indexes.

For this work, several simplifying assumptions were proposed to convert the former steady-state model to a dynamic model suitable for optimization purposes. In the context of the dynamic optimization of the whole plant, the main quantities to be provided by the model were monomer conversion, temperature, component compositions and number average molecular weight (Mn). This last quantity represents the average mass of monomer incorporated to each mole of polymer product.

At this step, the main objectives were to keep the size of the optimization problem small and to ensure that the same steady-state condition is obtained in the dynamic model.

The reactions that only affect molecular properties other than Mn were not considered at this stage of the work because they do not affect the grade change optimization. The final selected kinetic mechanism was:

Peroxide indication

$$I_l \xrightarrow{k_{\mathrm{dl}}} 2\,R(0); \quad l = 1, 2$$

Oxygen initiation

$$\mathrm{O_2} + \mathrm{M} \xrightarrow{k_o} 2\,R(0)$$

Propagation

$$R(x) + \mathrm{M} \xrightarrow{k_{\mathrm{p}}} R(x+1)$$

Termination by combination

$$R(x) + R(y) \xrightarrow{k_{\mathrm{tc}}} P(x+y)$$

Thermal degradation

$$R(x+1) \xrightarrow{k_{\mathrm{tdt}}} P(x) + R(0)$$

Chain transfer to butane (S)

$$R(x) + S \xrightarrow{k_{\mathrm{trs}}} P(x) + R(0)$$

where I_l, jth initiator; k, kinetic constants; M, ethylene; $P(x)$, polymer molecules which contain 'x' monomer units; $R(x)$, radical molecules which contain 'x' monomer units.

The Arrhenius law was used to describe the dependence of kinetic constants with temperature and pressure. The values of preexponential factors and activation energies may be found elsewhere (Brandolin et al., 1996; Asteasuain, Pereda, Lacunza, Ugrin, & Brandolin, 2000).

Four additional chemical species are considered *only* in the reactor model. The oxygen ($j = 5$) and peroxide initiators ($j = 7$) are injected to the reactor and consumed totally there. Radicals ($j = 8$) are generated and consumed only in the reactor. Besides, polymer ($j = 6$) mass fraction only appears in reactor balances.

The reactor was divided in six jacket sections, according to their thermal levels. The first section is used to preheat the reaction mixture up to the temperature where oxygen initiates the reaction. In the second section, radicals generated by oxygen propagate. Two different peroxide initiators are injected at the beginning of the third and fifth sections generating two reaction zones respectively. The fourth and sixth sections are used for cooling the reacting mixture. Each of these sections is modeled as a plug flow reactor. To reduce the number of algebraic variables we used uniform global heat transfer coefficients, specific heat, density, jacket temperature, and jacket pressure at each section. No balances for the jacket side were necessary. To simplify pressure calculations on the reaction side we used information from the rigorous model to propose a linear variation of pressure along the reactor.

Further simplifications were necessary in the case of peroxide and radicals balances, in order to obtain consistency between stationary predictions of the dynamic model and its corresponding steady state model. The assumption of quasi-stationary state was applied for both radicals and peroxides, so the time derivatives disappear from the respective balance equations. Nevertheless, a time variation is observed in the resulting concentrations due to temperature dependence of kinetic constants.

Finally, the following dynamic equations are applied for each one of the jacket sections ($k = 1, 6$) in which the reactor was divided:

Temperature equation

$$\left.\frac{\partial T(z,t)}{\partial t}\right|_k = \frac{1}{\rho(k)C_p(k)}\left\{ - v(k)\rho(k)C_p(k)\left.\frac{\partial T(z,t)}{\partial z}\right|_k \right. \tag{3}$$

$$+ (- k_p(z,t)w^8(z,t)\rho(k)w^1(z,t)\frac{\rho(k)}{M_{mon}}(- \Delta H)$$

$$\left. - 4U(k)(T(z,t) - T_j(k))/(D_i)\right\}.$$

Ethylene (w^1) balance

$$\left.\frac{\partial w^1(z,t)}{\partial t}\right|_k = - v(k)\left.\frac{\partial w^1(z,t)}{\partial z}\right|_k$$

$$- k_p(z,t)w^8(z,t)\rho(k)w^1(z,t)$$

$$- k_0(z,t)w^5(z,t)^{1.1}\frac{\rho(k)^{1.1}}{M_{ox}^{1.1}}w^1(z,t)\ . \tag{4}$$

Butane (w^2) balance

$$\left.\frac{\partial w^2(z,t)}{\partial t}\right|_k = - v(k)\left.\frac{\partial w^2(z,t)}{\partial z}\right|_k$$

$$- k_{trs}(z,t)w^8(z,t)\rho(k)w^2(z,t). \tag{5}$$

Oxygen (w^5) balance

$$\left.\frac{\partial w^5(z,t)}{\partial t}\right|_k = - v(k)\left.\frac{\partial w^5(z,t)}{\partial z}\right|_k$$

$$- k_0(z,t)w^5(z,t)^{1.1}\frac{\rho(k)^{0.1}}{M_{ox}^{0.1}}w^1(z,t)\frac{\rho(k)}{M_{mon}}. \tag{6}$$

Global polymer (w^6) balance

$$\left.\frac{\partial w^6(z,t)}{\partial t}\right|_k = - v(k)\left.\frac{\partial w^6(z,t)}{\partial z}\right|_k$$

$$- 0.5k_{tc}(z,t)w^8(z,t)^2\rho(k)$$

$$- k_{trs}(z,t)w^2(z,t)\frac{\rho(k)}{M_{but}}w^8(z,t)$$

$$+ k_{tdt}(z,t)w^8(z,t). \tag{7}$$

Peroxide (w^7) balances

$$0 = - v(k)\left.\frac{\partial w^{7,l}(z,t)}{\partial z}\right|_k - k_{dl}(z,t)w^{7,l}(z,t) \quad \ell = 1,2. \tag{8}$$

Radical (w^8) balances

$$0 = - v(k)\left.\frac{\partial w^8(z,t)}{\partial z}\right|_k + \sum_{l=1}^{2} 2k_{dl}(z,t)w^{7,l}(z,t)/M_{in,l}$$

$$- k_0(z,t)w^5(z,t)^{1.1}\frac{\rho(k)^{1.1}}{M_{ox}^{1.1}}w^1(z,t)/M_{mon}$$

$$+ k_{tc}(z,t)w^8(z,t)^2\rho(k) \tag{9}$$

where C_p, specific heat (J/mol K); D_i, internal diameter (m); M_{but}, butane molecular weight; $M_{in,l}$, 'jth' initiator molecular weight; M_{mon}, monomer molecular weight; M_{ox}, oxygen molecular weight; T, temperature (K); T_j, jacket fluid temperature (K); U, global heat transfer coefficient (J/m^2 s K); v, axial velocity (m/s); ΔH, heat of polymerization (J/mol).

The initial and boundary conditions may be expressed as:

Initial conditions

$$t = 0 \quad \begin{array}{l} w^j(z,0) = w_0^j(z) \\ T(z,0) = T_0(z). \end{array} \tag{10}$$

Boundary conditions

$$z = 0 \quad \begin{array}{l} w^j(0,t) = w^j_{z=0} \\ T(0,t) = T_{z=0} \end{array} \tag{11}$$

where $j = 1, 2, 5–8$.

The dimensional variables were converted to a proper dimensionless form. In general the concentrations and temperature were divided by a factor about the same order of magnitude of the corresponding variable. This approach worked well for all the variables except for oxygen. This problem was solved by taking the logarithm of the dimensionless oxygen concentration.

To incorporate this model to the optimization framework, the space coordinate z was discretized using backward finite differences. This spatial discretization was not uniform; shorter intervals were taken after initiator injections since the rate of change of the variables increases significantly.

The resulting ordinary differential equations were coupled with the rest of plant equations and solved by orthogonal collocation on finite elements as described in the following sections.

3. Dynamic optimization problem

In this type of plant, a common practice to infer the final product quality is to measure the composition of butane in the low-pressure recycle stream. Therefore, as a performance criterion for the dynamic optimization problem, we selected the deviation of this variable respect to the desired set point.

In order to account for the minimum switching time between two steady states, the time weighted integral error function was selected as the objective function. As the manipulated variable, the butane feed and the purge stream profiles are used.

$$\min \int_0^{t_f} (x_{bu} - x_{bu}^{set})^2 dt \tag{12}$$

s.t. DAE Model $(1-11)$

$$\boldsymbol{z}(t=0) = \boldsymbol{z}^0$$

$$\boldsymbol{z}^l \le \boldsymbol{z} \le \boldsymbol{z}^u$$

$$\boldsymbol{y}^l \le \boldsymbol{y} \le \boldsymbol{y}^u$$

$$u^l \le u \le u^u$$

where $\boldsymbol{z}$ is the vector of differential variables, $\boldsymbol{y}$ is the vector of algebraic variables and u is the control variable which represents the butane feed to the plant. Adding a new differential variable to the problem we can write it in Mayer form, where the objective function becomes:

$$\min\ z_{\text{new}}(t_f) \tag{13}$$

and the following two constraints have been added in Eq. (12)

$$\dot{z}_{\text{new}} = (x_{\text{bu}} - x_{\text{bu}}^{\text{set}})^2$$

$$z_{\text{new}}(0) = 0$$

The continuous state and control variables are discretized, by applying orthogonal collocation on finite elements and the resulting NLP is solved with a decomposed barrier (or interior point) algorithm. In the remainder of this section we briefly present the basic characteristics of the discretization approach and the barrier algorithm.

3.1. Discretization

The continuous dynamic optimization problem is discretized by applying collocation of finite elements. We use a monomial basis representation for the differential profiles.

$$z(t) = z_{i-1} + (t - t_{i-1}) \sum_{q=1}^{\text{ncol}} \Omega_q\left(\frac{t - t_{i-1}}{h_i}\right) \frac{\mathrm{d}z}{\mathrm{d}t_{i,q}} \tag{14}$$

where z_{i-1} is the value of the differential variable at the beginning of element i, $h_i = (t_i - t_{i-1})$ is the length of element i, $\mathrm{d}z/\mathrm{d}t_{i,q}$ is the value of its first derivative in element i at the collocation point q, and Ω_q is a polynomial of order ncol.

The control and algebraic variables are approximated by:

$$y(t) = \sum_{q=1}^{\text{ncol}} \psi_q\left(\frac{t - t_{i-1}}{h_i}\right) y_{i,q} \tag{15}$$

$$u(t) = \sum_{q=1}^{\text{ncol}} \psi_q\left(\frac{t - t_{i-1}}{h_i}\right) u_{i,q} \tag{16}$$

where $y_{i,q}$ and $u_{i,q}$ represent the values of the algebraic and control variables, respectively, in element i at collocation point q. Here, ψ_q is a Lagrange polynomial of order ncol. The differential variables are required to be continuous throughout the time horizon, while the control and algebraic variables are allowed to have discontinuities at the boundaries of the elements. Fixing the number and the length of the elements, and the number of collocation points the substitution of Eqs. (14)–(16) into Eq. (12) leads to the following NLP.

$$\min\quad f(\boldsymbol{x}) \tag{17}$$

$$\text{s.t.}\quad c(\boldsymbol{x}) = 0 \tag{18}$$

$$\boldsymbol{x}^l \le \boldsymbol{x} \le \boldsymbol{x}^u$$

where $\boldsymbol{x}$ is the vector of discretized variables

$$\boldsymbol{x} = \begin{bmatrix} z_i & \dfrac{\mathrm{d}z_{i,q}}{\mathrm{d}t} & y_{i,q} & u_{i,q} \end{bmatrix}^T \tag{19}$$

3.2. Barrier method

The NLP problem, Eqs. (17)–(19) is solved using a reduced space barrier method (Cervantes, Waechter, Tutuncu & Biegler, 2000). This method has proved to be very efficient for solving DAE optimization problems, especially when the dimension of the state variables is much larger than that of the control variables. The method also adds robustness to the solution procedure by performing local factorizations. This allows us to preserve and exploit the structure of the problem and to detect ill-conditioning due to unstable modes in the DAE system.

Without loss of generality and in order to simplify the presentation of the algorithm the NLP problem Eqs. (17) and (18) can be written as:

$$\min\quad f(\boldsymbol{x}) \tag{20}$$

$$\text{s.t}\quad c(\boldsymbol{x}) = 0 \tag{21}$$

$$\boldsymbol{x} \ge 0.$$

This approach replaces the bound constraints with a logarithmic barrier term, which is added to the objective function. The problem can be written as:

$$\min\quad \varphi_\mu(x) = f(x) - \mu \sum_{i=1}^{n} \ln(x^i) \tag{22}$$

$$\text{s.t}\quad c(x) = 0. \tag{23}$$

where $\mu > 0$ is a barrier parameter. The degree of influence of the barrier is determined by the size of μ. Thus, $x^*(\mu)$ converges to a local solution x^* of the original problem Eqs. (20) and (21) as μ goes to zero. Consequently, a strategy for solving the original NLP is to solve a sequence of barrier problems for decreasing barrier parameters μ. Since the exact solution $x^*(\mu)$ is not of interest for large μ, the corresponding barrier problem is solved only to a relaxed accuracy ε, and the approximate solution is then used as a starting point for the next barrier problem.

To solve Eqs. (22) and (23) with a fixed value of μ, we follow a primal–dual approach that generates search directions for primal variables $x > 0$ as well as for dual variables $v > 0$, which correspond to the Lagrange multipliers of the bound constraints in Eq. (21). The corresponding KKT system is:

$$\nabla f(x) + A(x)\ \lambda - v = 0 \tag{24}$$

$$\boldsymbol{XVe} - \mu \boldsymbol{e} = 0$$

$$c(x) = 0$$

where $A(x) = \nabla c(x)$, λ are the Lagrange multipliers of the equality constraints in Eq. (23), $\boldsymbol{e}$ denotes a vector of ones of appropriate dimension, and the diagonal matrices $\boldsymbol{X}$ and $\boldsymbol{V}$ are defined by $\boldsymbol{X} = \text{diag}\{x\}$ and $\boldsymbol{V} = \text{diag}\ \{v\}$. Note that Eq. (24) is modified in the sense that the corresponding equations in the 'traditional' KKT conditions are multiplied by $\boldsymbol{X}$.

If we solve this system of nonlinear equations with Newton's method, at an iterate (x_k, λ_k, v_k), the corresponding search direction would be obtained by solving:

$$\begin{bmatrix} H_k & A_k & -I \\ A_k^T & 0 & 0 \\ V_k & 0 & X_k \end{bmatrix} \begin{bmatrix} d_k^x \\ d_k^\lambda \\ d_k^v \end{bmatrix} = - \begin{bmatrix} \nabla f(x_k) + A_k \lambda_k - v_k \\ c(x_k) \\ \boldsymbol{X}_k \boldsymbol{V}_k \boldsymbol{e} - \mu e \end{bmatrix}$$

where H_k denotes the Hessian of the Lagrangian function for Eqs. (17) and (18). Reducing this linear system yields:

$$\begin{bmatrix} H_k + \Sigma_k & A_k \\ A_k^T & 0 \end{bmatrix} \begin{bmatrix} d_k^x \\ \lambda_k + d_k^\lambda \end{bmatrix} = - \begin{bmatrix} \nabla \varphi_\mu(x_k) \\ c_k \end{bmatrix}$$

and

$$d_k^v = \mu \boldsymbol{X}_k^{-1} \boldsymbol{e} - v_k - \Sigma_k\, d_k^x \tag{25}$$

where $\Sigma_k = \boldsymbol{X}_k^{-1}\ V_k$.

Obtaining d_k^x from Eq. (25) is equivalent to solving the quadratic problem

$$\begin{aligned} \text{Min} \quad & \nabla \varphi_\mu^T d^x + \tfrac{1}{2} d^{xT} (H_k + \Sigma_k) d^x \\ s.t. \quad & c(x_k) + A_k^T d^x = 0 \end{aligned} \tag{26}$$

as long as $(H_k + \Sigma_k)$ is positive definite in the null space of A_k^T. The similarity of this QP to the one used in rSQP in our earlier studies, in particular with reduced space Quasi-Newton updates, allows us to solve each barrier problem with a reduced space approach, where the overall step is partitioned into a range and null space component. For this, the variables are partitioned into m dependent and $(n-m)$ independent variables. With this partition A^T takes the form $A^T = [\mathbf{C}\ \mathbf{N}]$ where $\mathbf{C}$ is a nonsingular $m \times m$ matrix and $\mathbf{N}$ is an $m \times (n-m)$ matrix. The search direction d^x at each iteration k can be written as:

$$d_k = R_k d_R + \boldsymbol{Q}_k d_Q \tag{27}$$

where the matrix $\boldsymbol{Q}$ satisfies $A_k^T \boldsymbol{Q}_k = 0$ and. Q_k and R_k are chosen as

$$\boldsymbol{Q}_k = \begin{bmatrix} -C(x_k)^{-1} N(x_k) \\ I \end{bmatrix} \quad \text{and} \quad R_k = \begin{bmatrix} I \\ 0 \end{bmatrix} \tag{28}$$

The range space direction, d_R, is obtained from

$$d_R = -\boldsymbol{C}_k^{-1} c_k \tag{29}$$

and the null space direction, d_Q, is obtained by solving the following QP subproblem:

$$\begin{aligned} & \min_{d_Q \in \Re^{n-m}} \left(\boldsymbol{Q}_k^T \nabla \varphi_\mu(x_k) + \boldsymbol{Q}_k^T \textstyle\sum_k R_k d_R \right)^T d_Q \\ & + \tfrac{1}{2} d_Q^T \left(\boldsymbol{Q}_k^T \left(H_k + \textstyle\sum_k \right) \boldsymbol{Q}_k \right) d_Q \end{aligned} \tag{30}$$

The solution of this QP, which is unconstrained, can be obtained directly as:

$$\begin{aligned} d_Q = & -\left(\boldsymbol{Q}_k^T \left(H_k + \textstyle\sum_k \right) \boldsymbol{Q}_k \right)^{-1} \\ & \left(\boldsymbol{Q}_k^T \nabla \varphi_\mu(x_k) + \boldsymbol{Q}_k^T \textstyle\sum_k R_k d_R \right) \end{aligned} \tag{31}$$

where the term $\boldsymbol{Q}_k^T H_k \boldsymbol{Q}_k$, is approximated with a Quasi-Newton method. After the step d_k^x is computed, an Armijo line search is performed using a special-purpose, primal–dual l_1 penalty function. Details of this algorithm along with an extensive performance evaluation are given in Cervantes et al. (2000).

3.3. Mesh refinement for optimal control

To improve on the accuracy of the optimal state and control problems, we also apply a mesh refinement strategy to this problem. Mesh refinement is governed primarily by accuracy and the optimal location of the control variable breakpoints. By introducing the element lengths, h_i, as variables and aggregating the variable bounds as inequality constraints, the nonlinear programming problem in Eqs. (17)–(19) can easily be extended to mesh refinement for optimal control. Here we consider element lengths as decision variables, error constraints can be imposed in each finite element and a larger nonlinear problem is solved. The error constraints guarantee the accuracy of the discretization while variable elements lengths locate the optimal breakpoints of the control variables. The main difficulties of this approach are that the resulting NLP problem is more nonlinear than with fixed elements, and the error constraints induce inconsistencies in the linearization if the problem is poorly initialized. To overcome this difficulty, Tanartkit and Biegler (1997) proposed a bi-level strategy in which the solution of an outer problem determines the element lengths. Then, the solution of an inner problem (fixed mesh) determines the control and state variables. With this approach, the solution of a highly nonlinear problem is avoided. However, the outer problem is nonsmooth because the active constraints sets in the inner problem can change from one mesh to another. In Biegler, Cervantes, and Waechter (2001), we develop a new

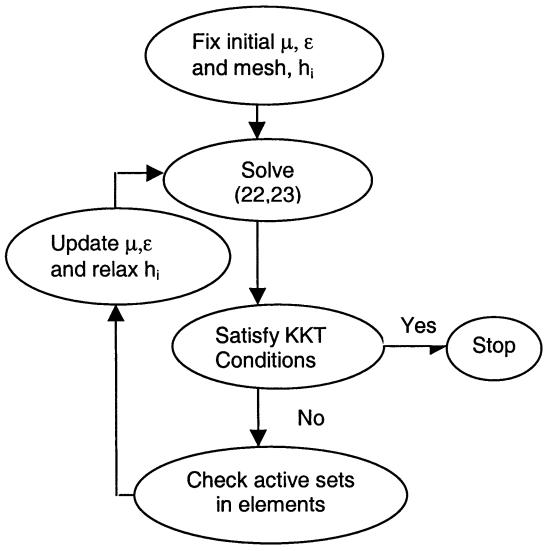

Fig. 2. Mesh refinement algorithm.

Table 1
Steady state conditions

Ethylene flow rate	12334 kg/h
Butane flow rate	12 kg/h
Purge flow rate	355 kg/h
Butane composition	0.0205
Low-pressure recycle	

approach that overcomes problems with nonsmoothness by embedding the mesh refinement within the interior point algorithm, as seen in Fig. 2.

The main concept for mesh refinement algorithm is to detect active constraints during the solution procedure and obtain a solution where the active set does not change within any finite element. As shown in Biegler et al. (2001) an active constraint set that remains constant in each of the finite elements is necessary to determine an (arbitrarily) accurate optimal control profile. As seen in Fig. 2, we solve the barrier problem Eqs. (22) and (23) for a given μ to given tolerance ε, proportional to μ. At these intermediate solutions, we check each element for changes in active constraints within an element. If there are changes in active sets between two consecutive elements, we free the element length, h_i, between them as a new variable in the barrier problem. We then decrease μ and $\varepsilon \propto \mu$ according to the barrier method algorithm in Cervantes et al. (2000) and repeat the process until the method converges.

Upon convergence, we then check two additional criteria to determine if a sufficient number of elements is used. First, approximation error constraints for the state profiles need to be imposed and satisfied.

Second, from optimal control theory, the Hamiltonian function should remain constant for the whole time horizon. Here, for the DAE system:

$$\dot{z} = F(z, y, u)$$
$$G(z, y, u) = 0 \tag{32}$$

we can define adjoint variables $\lambda(t)$ and $\gamma(t)$, and write the Hamiltonian function as:

$$H(t) = \lambda(t)^T\ F(t) + \gamma(t)^T\ G(t). \tag{33}$$

This function can be evaluated at each collocation point and adjoint variables are related to the KKT multipliers at the solution of the NLP Eqs. (22) and (23).

According to our experience, a good initial mesh selection with a sufficient number of elements usually satisfies these two criteria. If not, additional elements are inserted at locations where these criteria are most violated and the algorithm in Fig. 2 is repeated. Detailed derivation and presentation of the algorithm, the error and Hamiltonian criteria and applications to optimal control problems can be found in Biegler et al. (2001).

4. Results

The above plant model together with the time delays and the detailed reactor model, leads to a system with 532 differential-algebraic equations. To capture the dynamics of the reactor model adequately, three collocation points were required and up to 40 finite elements were needed in the discretization process. The resulting problem was solved using our interior point algorithm running on a DEC AlphaStation 500 workstation.

In this work we analyze two different product grade transitions (cases 1 and 2), to show the capabilities of the developed large-scale optimization model. Case 1 corresponds to a decrease while case 2 corresponds to an increase in molecular weight. In all cases, we started from the same initial steady state condition (see Table 1), corresponding to a conversion of 28.5%.

For case 1, 35 finite elements and three collocation points were required in the discretization process, leading to a nonlinear program with 73,425 variables. Here 154 iterations and 4366.2 CPUs were required by the interior point algorithm to achieve convergence.

Fig. 3 presents the optimal profile of the fresh butane flow that minimizes the transition time from the initial to a final steady state, which is characterized by a polymer of lower molecular weight. The other operating process conditions remained unchanged. It is observed from the figure that the optimal profile for the butane flow is almost a piecewise constant function, consisting of taking the initial steady state flow to its upper bound, keeping it there for 0.8 h and then lowering it to its final steady state value. This manipulation produces a linear increase in the concentration of butane in the low-pressure recycle and leads to an

increment of butane concentration in the reactor that favors chain transfer reactions. These reactions are responsible for the decrease in average molecular weight. As can be seen in Fig. 3, the model predicts much faster reactor dynamics than that of the global plant, as is usually the case in actual plants.

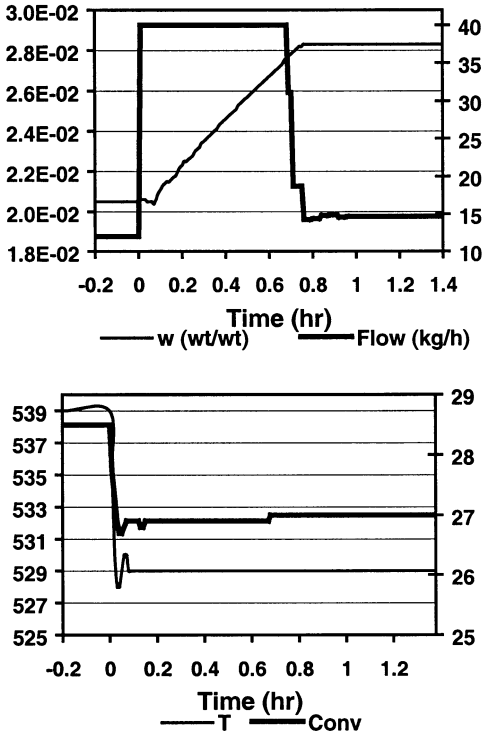

Fig. 3. Optimal control and state profiles: case 1.

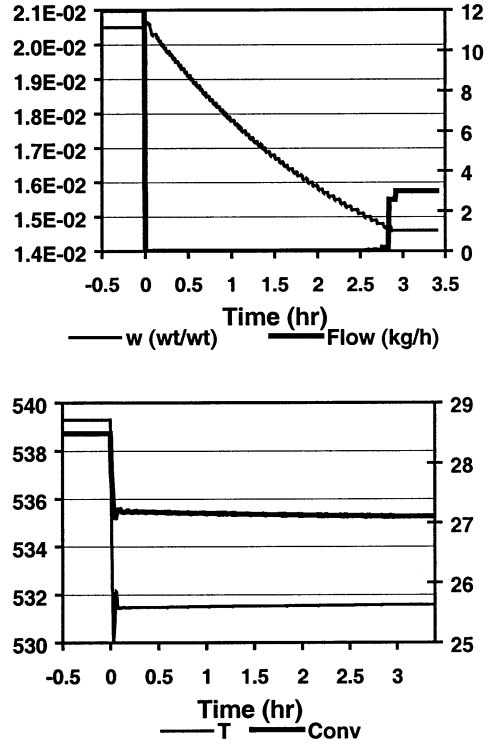

Fig. 4. Optimal control and state profiles: case 2.

In case 2, we seek a transition to increase the molecular weight. A number of 40 finite elements and three collocation points were required, leading to a nonlinear program with 83,845 variables. The interior point algorithm required 126 iterations and 3728.4 CPUs for convergence.

Fig. 3 shows that the optimum butane flow profile that leads to an increase in molecular weight must start at a low value for more than 2.5 h and then increases to its final steady state value. This manipulation produces a linear decrease in butane concentration in the low-pressure recycle. Butane composition also decreases in the reactor making the chain transfer reaction less significant; the product molecular weight increases accordingly.

The time delay effects on the process variable profiles are evident for both cases from Figs. 3 and 4.

For both cases, a large part of the computation times are taken up not by the NLP algorithm but in the calculation of the derivative information for the reactor and plant models. For this study, the Jacobian matrices were obtained by finite difference perturbations. More efficient strategies for obtaining exact derivatives will be considered in future work.

The optimal control policies presented above lead to a significant savings in transition times. The transition time in the actual plant is about 5 h and the corresponding process dynamics were also in excellent agreement with the overall plant model Eqs. (1) and (2) (see Schbib et al., 1992). Using the optimal profiles presented here we were able to reduce this transition time to no more than 2.8 h. Applied at each grade transition, this translates to a reduction of at least 23 tons of off-spec product using the plant model.

4.1. Optimal control with simplified model

We also compare the results of case 1 with a simplified reactor model where the reactor was treated as a black box with the conversion fixed at a value obtained from plant data. It is interesting to note that the optimal control policies with the incorporation of the reactor model are very close to those with a fixed conversion reactor model, as shown below in Fig. 5. With the simplified reactor, the model has 156 differential equations and 64 algebraic equations; it was discretized with three collocation points on 15 finite elements, resulting in an NLP with 12,396 variables and 12,366 equality constraints. The NLP algorithm obtains an optimal solution in 81 iterations and 418.1 CPUs.

As seen in Fig. 5, the profiles are similar to the ones presented in Fig. 3 with the more rigorous model. This is due to the fact that the time constant of the reactor is much faster than that of the overall process. As a

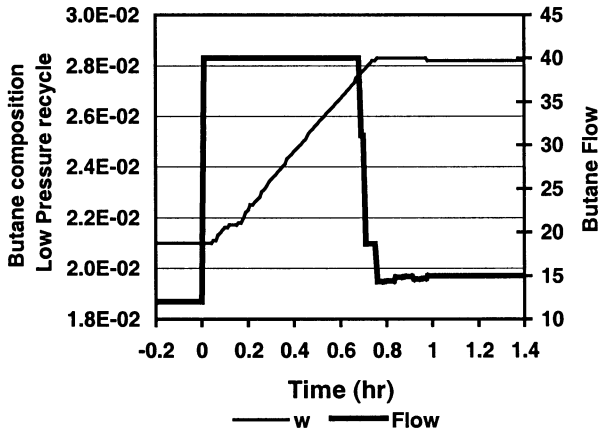

Fig. 5. Optimal control profiles: using the simplified model for case 1.

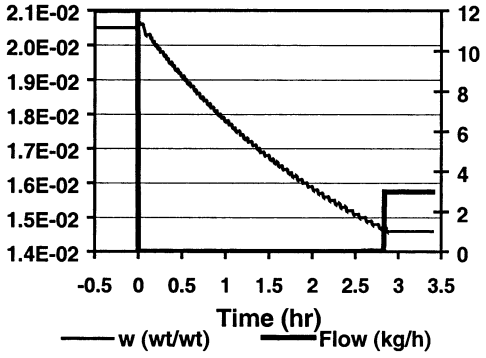

Fig. 6. Optimal control profiles after mesh refinement for case 2.

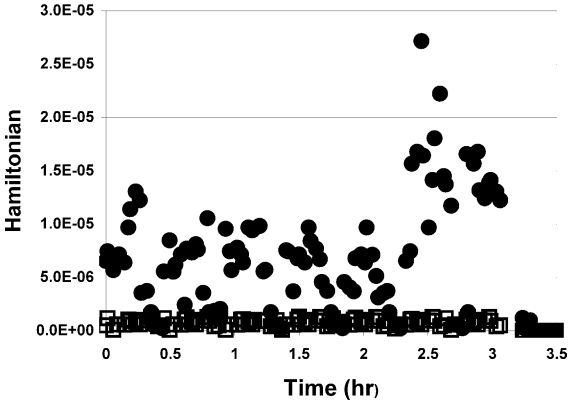

Fig. 7. Comparison of Hamiltonians for mesh refinement in case 2. (closed dots—fixed mesh; open squares—with mesh refinement).

result, detailed reactor dynamics play a much smaller role in the optimization than those of the process. On the other hand, the detailed reactor model is able to predict appropriately the actual steady state reactor behavior for a wider range of operating conditions, especially with respect to the steady state. Consequently, it improves the model predictive capabilities for key plant variables such as conversion, temperature profiles and molecular weights.

4.2. Adjustment of finite elements

Finally, we apply the mesh refinement approach in Section 3 to the low density polyethylene results of case 2, which corresponds to an increase in molecular weight. For this case 40 finite elements and three collocation points were used, leading to a nonlinear program with 83,845 variables. To find an optimal placement of finite elements, the modified interior point algorithm with mesh refinement required 174 iterations and 5,407.1 CPUs. Fig. 6 shows the control profiles for this case. Compared to Fig. 4, we see that the finite elements are now placed to ensure a sharp transition in the control policy.

As mentioned in Section 3, autonomous dynamic optimal control problems require that the Hamiltonian function be constant over time. This function is calculated as part of the mesh refinement and the effect can be seen in Fig. 7, where profiles from Fig. 4 (fixed mesh) and Fig. 6 (with mesh refinement) are compared. In the latter case the optimal control profile is quite accurate, as time fluctuations in the Hamiltonian are less than 10^{-6}. Thus, no additional improvement of these control profiles can be achieved through further refinement of the mesh or addition of finite elements.

5. Conclusions

Optimal control policies are derived for grade transition problems for a large-scale LDPE plant model. Using orthogonal collocation on finite elements to represent the DAE model and a novel interior point method for solving the resulting nonlinear program, we obtain the solution of problems with over 80,000 variables. Moreover, the resulting solutions lead to a reduction in the transition time (and of off-spec LDPE product) of over 44%. In addition, a mesh refinement strategy has been implemented that leads to a constant Hamiltonian profile for the dynamic optimization. These results show that further improvements in the control profiles cannot be achieved with additional finite elements or mesh refinement. Future work will deal with more efficient model formulations, accurate gradient calculations from the model and large-scale extensions to this plant.

Acknowledgements

PLAPIQUI's authors acknowledge the financial support of CONICET (the National Research Council of Argentina) and UNS (Universidad Nacional del Sur). CMU's authors gratefully acknowledge a fellowship for Arturo Cervantes from the Universidad Nacional Autonoma de Mexico and support from the US National Science Foundation.

References

Asteasuain, M., Pereda S., Lacunza, M. H., Ugrin, P. E., & Brandolin A. (2001). Industrial high-pressure ethylene polymerization initiated by peroxide mixtures: a reduced mathematical model for parameter adjustment, *Polym. Eng. Sci. 41*(5), 711–726.

Biegler, L. T., Cervantes A., & Waechter A. (2001) Advances in Simultaneous Strategies for Dynamic Process Optimization, submitted for publication.

Brandolin, A., Lacunza, M. H., Ugrin, P. E., & Capiati, N. J. (1996). High-pressure polymerization of ethylene. An improved mathematical model for industrial tubular reactors. *Polym. Reac. Eng.*, *4*, 193–241.

Cervantes, A., Tonelli S., Bandoni, J. A., & Biegler L. (1998). Optimal switching between steady states in low density polyethylene plant, Paper 236g, *Annual AIChE meeting*, Miami Beach, FL.

Cervantes, A., Waechter, A., Tutuncu, R., & Biegler, L. T. (2000). A reduced space interior point strategy for optimization of differential algebraic systems. *Computers and Chemical Engineering*, *24*, 39–51.

Lacunza, M. H., Ugrin, P. E., Capiati, N. J., & Brandolin, A. (1998). Heat transfer coefficient in a high-pressure tubular reactor for ethylene polymerization. *Polym. Eng. Sci.*, *38*, 992–1013.

Schbib, S., Tonelli, S., Brignole, E., & Romagnoli, J. (1992). Linearized dynamic model of an industrial low density polyethylene plant. *Computers and Chemical Engineering*, *17S*, S323–S328.

Tanartkit, P., & Biegler, L. T. (1997). A nesteed simultaneous approach for dynamic optimization problems-II: the outer problem. *Computers and Chemical Engineering*, *21*(12), 1365.